

楊叔子科技論文選

(下)

涂又光題

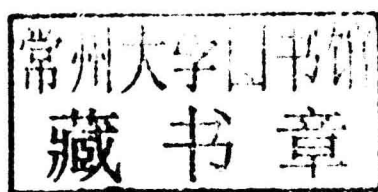


華中科技大学出版社
<http://www.hustp.com>

楊叔子科枝論文選

(下)

涂又光題



楊叔子

图书在版编目(CIP)数据

杨叔子科技论文选(上、下)/杨叔子. —武汉: 华中科技大学出版社, 2012. 9
ISBN 978-7-5609-8363-9

I. 杨… II. 杨… III. 机械学-文集 IV. TH11-53

中国版本图书馆 CIP 数据核字(2012)第 209443 号

杨叔子科技论文选(上、下)

杨叔子

策划编辑: 熊新华 杨 玲

责任编辑: 包以健

责任校对: 张 琳

责任监印: 周治超

出版发行: 华中科技大学出版社(中国·武汉)

武昌喻家山 邮编: 430074 电话: (027)81321915

录 排: 华中科技大学惠友文印中心

印 刷: 湖北新华印务有限公司

开 本: 710mm×1000mm 1/16

印 张: 38 插页: 4

字 数: 675 千字

版 次: 2012 年 9 月第 1 版第 1 次印刷

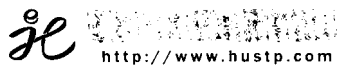
定 价: 100.00 元(含上、下册)



本书若有印装质量问题,请向出版社营销中心调换

全国免费服务热线: 400-6679-118 竭诚为您服务

版权所有 侵权必究



<http://www.hustp.com>

中国·武汉

目录

三支承主轴部件静刚度的分析与讨论 /1
δ 函数在机械制造中的应用 /19
A Study of the Static Stiffness of Machine Tool Spindles /30
平稳时间序列的数学模型及其阶的确定的讨论 /57
时序建模与系统辨识 /64
金属切削过程颤振预兆的特性分析 /74
机械设备诊断学的探讨 /86
灰色预测和时序预测的探讨 /97
Quantitative Wire Rope Inspection /106
钢丝绳断丝定量检测的原理与实现 /116
复杂系统诊断问题的研究 /126
Plant Condition Recognition—A Time Series Model Approach /136
Space-domain Feature-based Automated Quantitative Determination of Localized Faults in Wire Ropes /150
基于深知识的多故障两步诊断推理 /168
机床切削系统的强迫再生颤振与极限环 /176
机械设备诊断学的再探讨 /185
机械设备诊断策略的若干问题探讨 /194
Forced Regenerative Chatter and its Control Strategies in Machine Tools /201
智能制造技术与智能制造系统的发展与研究 /212
两类小波函数的性质和作用 /220
Intelligent Prediction and Control of a Leadscrew Grinding Process Using Neural Networks /233
大直径钢丝绳轴向励磁磁路的研究 /244
金属切削机床切削噪声的动力学研究 /250
BP 网络的全局最优学习算法 /263
基于神经网络的结构动力模型修改和破损诊断研究 /268

- A CORBA-based Agent-driven Design for Distributed Intelligent Manufacturing Systems /275
- 内燃机气缸压力的振动信号倒谱识别方法 /295
- A Novel Co-based Amorphous Magnetic Field Sensor /302
- 基于高阶统计量的机械故障特征提取方法研究 /312
- 基于因特网的设备故障远程协作诊断技术 /318
- 磁性无损检测技术中磁信号测量技术 /323
- 分布式网络化制造系统构想 /332
- 网络化制造与企业集成 /342
- 磁性无损检测技术中的信号处理技术 /351
- Intelligent Machine Tools in a Distributed Network Manufacturing Mode Environment /362
- AR 模型参数的 Bootstrap 方差估计 /387
- 虚拟制造系统分布式应用研究 /392
- Wigner-Ville 时频分布研究及其在齿轮故障诊断中的应用 /400
- 先进制造技术及其发展趋势 /409
- Feature Extraction and Classification of Gear Faults Using Principal Component Analysis /420
- 制造系统分布式柔性可重组状态监测与诊断技术研究 /434
- 基于 Markov 模型的分布式监测系统可靠性研究 /444
- 再论先进制造技术及其发展趋势 /456
- 基于神经网络信息融合的铣刀磨损状态监测 /464
- 以人为本——树立制造业发展的新观念 /472
- 走向“制造-服务”一体化的和谐制造 /480
- Kinematic-parameter Identification for Serial-robot Calibration Based on POE Formula /491
- 高端制造装备关键技术的科学问题 /524
- 后记 /536
- 论文附录 /541

内燃机气缸压力的振动信号倒谱识别方法

刘世元 李锡文 杜润生 杨叔子

提 要 分析了内燃机缸盖系统的传递特性,提出了利用缸盖表面振动信号识别气缸压力的倒谱分析方法。通过倒谱开窗并进行平滑处理,使测量的振动信号和计算的传递函数更具鲁棒性,可以消除传感器测点位置和内燃机运行工况等敏感因素的影响。实验及分析结果表明了这种方法的可行性和有效性。

关键词:内燃机,气缸压力,振动,倒谱分析

目前,测量气缸压力的方法是在内燃机气缸盖上打孔,用压力传感器直接进行测量,但这种测量方法难以投入实际应用。内燃机表面振动信号的获取则方便可靠,通过适当处理可以用于识别和反演气缸压力。一种简单的方法是设计一个逆滤波器^[1],其值是缸盖传递函数的倒数。利用这种逆滤波器法获得的传递函数,只要幅值低点存在微小的变化,都将导致反演信号的严重失真。由于振动弹性波在传递通道间的消散和混响^[2],测量的振动信号及由此获得的传递函数易于受传感器安装位置和内燃机运行工况等敏感因素的影响^[3]。

本文提出倒谱变换及开窗处理的方法,获得平滑且具鲁棒性的传递函数,用于气缸压力信号的识别。这种方法消除了上述敏感因素的影响,为内燃机工作过程的振动诊断奠定了基础。

1 内燃机缸盖振动特性

工作状态下内燃机缸盖系统主要承受的激励源有5个:进、排气门开启和关闭的4个冲击力以及缸内气体压力。可以认为这些激励源彼此之间是线性无关的,缸盖系统简化为一个多输入、单输出的线性系统^[4],其输入和输出关系满足:

$$a(t) = p(t) * h_g(t) + x_{v1}(t) * h_{v1}(t) + x_{v2}(t) * h_{v2}(t) \\ + x_{v3}(t) * h_{v3}(t) + x_{v4}(t) * h_{v4}(t) + n(t)$$

式中, $a(t)$ 为缸盖表面振动信号; $p(t)$ 为气缸压力信号; $x_{v1}(t) \sim x_{v4}(t)$ 分别为进气门开启、排气门关闭、进气门关闭和排气门开启的激励信号; $h_g(t), h_{v1}(t) \sim h_{v4}(t)$ 分别为缸盖表面对上述各激励信号的响应函数; $n(t)$ 为噪声信号。对多缸内燃机而言, 各缸按一定的发火顺序依次工作, 缸盖振动响应是各缸响应的总和。

上述各激励信号之间具有严格的相位关系, 而且进、排气门开启的激励信号很小, 可以在时域内进行分离。对于气缸压力的识别和反演问题, 只取燃爆上死点附近的一段信号进行分析是可行的, 此期间也不存在进、排气门关闭激励。

2 气缸压力的倒谱识别方法

在燃爆上死点附近, 只考虑 $a(t)$ 和 $p(t)$ 的关系有

$$a(t) = p(t) * h_g(t) \quad (1)$$

从 $a(t)$ 中识别和分离出 $p(t)$ 的过程, 实质上是一个解卷积的过程。时域解卷积是相当困难的, 一般转换为频域内进行, 即

$$A(f) = P(f)H_g(f) \quad (2)$$

式中, $A(f)$ 和 $P(f)$ 分别为 $a(t)$ 和 $p(t)$ 的傅里叶变换; $H_g(f)$ 为缸盖传递函数, 是 $h_g(t)$ 的傅里叶变换。在此基础上, 设计一个逆滤波器 $H_t(f)$, 其幅值是 $H_g(f)$ 幅值的倒数, 相位是 $H_g(f)$ 相位的负值, 即满足 $H_t(f) = 1/H_g(f)$ 。那么, 根据系统的输出信号就能准确地反演输入信号, 即 $A(f)H_t(f) = P(f)H_g(f)H_t(f) = P(f)$ 。获得 $P(f)$ 后, 再经傅里叶逆变换即得 $p(t)$ 。

在实际应用中, 如果逆滤波器通过传递函数的简单反转得到, 则传递函数幅值中若干尖锐的低点, 将成为逆滤波器幅值中同样尖锐的峰值。传递函数幅值的这些低点只要存在微小的变化, 都将在逆滤波器中放大, 并造成反演信号的严重失真。事实上, 振动传感器的安装位置、内燃机循环间波动和任何微小的测量误差, 都将对振动信号的测量产生影响, 进而严重影响传递函数的这些低点。因此, 为了消除这些敏感因素, 最好采用非线性逆滤波, 倒谱开窗是一种有效的实现方法^[3]。

时域信号 $x(t)$ 的复频谱为 $X(f)$, 其复倒谱 $C_x(\tau)$ 定义为复频谱的复对数的傅里叶逆变换:

$$C_x(\tau) = F^{-1}[\ln X(f)]$$

式中, $F^{-1}[\cdot]$ 表示进行傅里叶逆变换。频谱 $X(f)$ 包括幅值谱 $|X(f)|$ 和相位谱 $\phi(f)$:

$$X(f) = F[x(t)] = |X(f)| \exp(-j\phi(f))$$

式中, $F[\cdot]$ 表示进行傅里叶变换。倒谱也包括幅值倒谱 $C_x(\tau)$ 和相位倒谱 $C_\phi(\tau)$:

$$C_x(\tau) = C_{|x|}(\tau) + C_\phi(\tau)$$

式中, $C_{|x|}(\tau) = F^{-1}[\ln |X(f)|]$; $C_\phi(\tau) = F^{-1}[-j\phi(f)]$ 。式(1)的时域卷积运算和式(2)的频域乘积运算,在倒频域内变成了加法运算:

$$C_a(\tau) = C_h(\tau) + C_p(\tau)$$

对于任一具体的内燃机,都可以先进行实验,根据测得的 $p(t)$ 和 $a(t)$,通过倒谱变换得出其传递函数的倒谱 $C_h(\tau)$ 。此后,就可以在内燃机状态监测中利用已知的 $C_h(\tau)$,从测量的 $a(t)$ 中识别出 $p(t)$ 。具体方法是:先对 $a(t)$ 进行倒谱变换并开窗处理,减去 $C_h(\tau)$ 后得到气缸压力信号的倒谱 $C_p(\tau)$;接着进行傅里叶变换并取指数,得到气缸压力信号的频谱 $P(f)$;最后进行傅里叶逆变换,就获得了气缸压力信号的时域波形 $p(t)$ 。计算过程如图 1 所示,虚框内给出的是通过先期实验分析获取缸盖传递函数倒谱的过程。

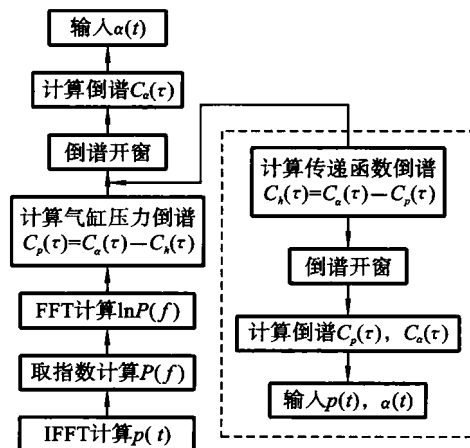


图 1 气缸压力波形的缸盖振动信号倒谱识别过程

3 实验与讨论

实验在一台四缸四冲程水冷柴油机(4135D-5型)上进行,发火顺序为1—3—4—2,缸径135 mm,行程150 mm,额定功率和额定转速分别为73.6 kW和1500 r/min。配气相位和喷油提前角(本文中的角度均指曲轴转角)如表1所示,它们为缸盖振动信号的识别提供重要依据。

表1 配气门相位和喷油提前角

进气门开启角	上止点前 $20^\circ \pm 6^\circ$
进气门关闭角	下止点后 $48^\circ \pm 6^\circ$
排气门开启角	下止点前 $48^\circ \pm 6^\circ$
排气门关闭角	上止点后 $20^\circ \pm 6^\circ$
喷油提前角	上止点前 $26^\circ \sim 29^\circ$

内燃机曲轴飞轮上装有磁电传感器,可以获取上止点参考信号;对第1缸缸盖打孔并安装石英压电传感器,可以测量气缸压力信号;第1缸缸盖上装有两个加速度传感器,分别靠近进气门和排气门,可以测量两个测点A和B处的振动信号。通过电荷放大器和高速多通道数据采集器,计算机对上述4路信号进行同步采集,每路的采样频率为50 Hz。

实验在额定转速1500 r/min下进行,图2是实际测量的时域波形。其中,(a)~(d)分别对应上述4路信号。结合表1所示的配气相位和喷油提前角,可以发现各激励信号确实可以在时域内进行分离。其中,对应燃爆压力段的缸盖振动

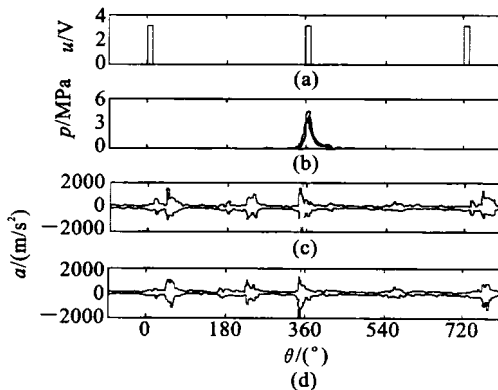


图2 气缸压力与缸盖振动时域波形

信号从开始喷油时明显增大, 约持续 90°曲轴转角。对于气缸压力的识别和反演问题, 可以从燃爆上死点前 30°处开始抽区间采样, 为便于使用快速傅里叶变换, 每次采样长度取为 512 个点, 相当于 10.24 ms 时间和 92.2°曲轴转角。

根据测点 A 处振动信号计算的缸盖传递函数如图 3 所示。其中: (a) 为采用频域方法直接计算的结果; (b) 和 (c) 为倒谱开窗处理后的结果, 开窗宽度分别为 64 和 32 个点, 采用简单的矩形窗, 保留低倒频率部分, 去掉高倒频率部分, 分别相当于去掉原时域信号中 1.28 ms 和 0.64 ms 的时延部分。结果表明, 频域计算得到的频谱中含有许多尖锐的低点和峰值; 进行倒谱开窗后, 这些低点和峰值变得平顺而光滑, 而且开窗宽度越窄, 频谱越光滑, 但也失去了频谱中的一些细节, 因此开窗宽度应权衡选择。

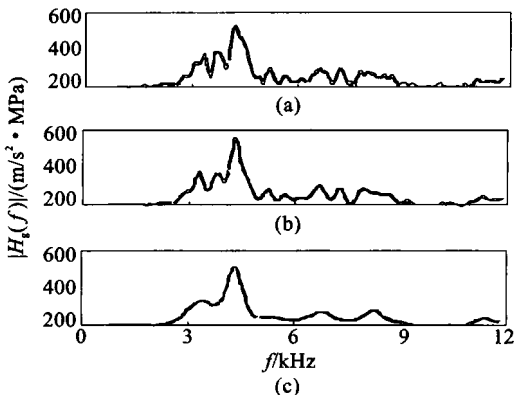


图 3 从测点 A 处获得的缸盖传递函数

获得缸盖传递函数的倒谱后, 就可以从其他表面振动的测量信号中识别出气缸压力。图 4 给出了用测点 A 处振动信号识别的气缸压力波形, 采用的传递函数倒谱是前期从测点 A 处获得的。图中, (a) 为实际测量结果, (b) 为采用逆滤波器法获得的结果, (c) 为倒谱开窗处理后的结果。

从图 4 中可以看出, 采用逆滤波器法时, 传递函数未经光滑处理, 识别的气缸压力波形与测量波形相差很大。相反, 经过倒谱开窗处理后获得的波形与测量波形则非常相近, 两者之间的误差是由于倒谱开窗处理造成的, 虽然因此失去了原测量压力波形中的某些细节成分, 但识别波形随时间变化的趋势依然明显, 可以进一步从中获取确定内燃机状态的信息。

此外, 利用测点 A 处先期获得的传递函数倒谱, 对测点 B 处振动信号也进行了气缸压力识别(图形略), 获得的识别波形与从测点 A 处获得的识别波形几乎相

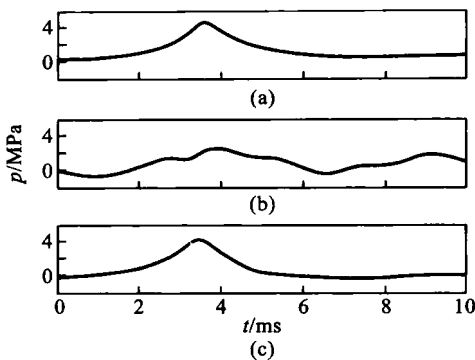


图 4 用测点 A 处振动识别的气缸压力

同,说明倒谱识别方法确实可以消除传感器测点位置等敏感因素的影响。

参 考 文 献

- [1] 郝志勇,舒歌群,薛远等. 内燃机气缸压力振动识别研究. 内燃机学报,1994,12(1):43~48.
- [2] 耿遵敏,宋孔杰,李兆前等. 关于柴油机振声特点及动态诊断方法的研究与探讨. 内燃机学报,1995,13(2):140~147.
- [3] Kim J T,Lyon R H. *Cepstral Analysis as a Tool for Robust Processing ,Reverberation and Detection of Transients*. Mechanical System and Signal Processing,1992,6(1):1~15.
- [4] 周铁尘,彭勇. 发动机缸盖系统振动特性研究. 内燃机学报,1988,6(1):49~56.

Identification of Engine Cylinder Pressure from Vibration Signals by Cepstral Analysis

Liu Shiyuan Li Xiwen Du Runsheng Yang Shuzi

Abstract A unique signal processing technique has been developed for identification of engine cylinder pressure from cylinder head vibration signals. By cepstral windowing, the smoothed and robust transfer function of cylinder head is obtained and will help to construct engine cylinder pressure. Experimental results in a real-world engine are presented and used to verify the theoretical developments. It is shown that this technique is practical to implement and provides the basis for engine diagnosis by vibration signals.

Keywords: Internal combustion engine, Cylinder pressure, Vibration, Cepstral analysis

(原载《华中理工大学学报(自然科学版)》1998年第26卷第6期)

A Novel Co-based Amorphous Magnetic Field Sensor

Haixia Zhang Yingjun Zhao Shuzi Yang Hejun Li

Abstract A novel Co-based amorphous magnetic field sensor was developed in this paper. It is a combination of two identical coils which are wrapped in one amorphous core, connected in anti-series, and they are induced by two identical pulse current sources. This structure is simple to construct and easy to optimize. Two optimizing methods: negative feedback coil and bias magnetic coil, greatly improved the sensors properties (linearity, sensitivity and dynamic range). At present, it is used in testing micro flaws in pipelines.

Keywords: Magnetic field sensor, Amorphous alloy, Negative feedback, Bias magnetic field

1 Introduction

Due to their superior soft magnetic properties, amorphous magnetic alloys have been considered as ideal active materials for high-performance magnetic sensors, such as MES (magnetoelastic sensors)^[1], MI (magneto-impedance) element^[2], and other kinds of sensor; these sensors play important roles in Non-destructive Testing (NDT). In our previous research, we paid more attention to pulse-induction amorphous magnetic field sensor^[3], which is simple and easy to operate. According to pick-up techniques, this kind of sensor can be divided into two types: the first one has single coil, which is supplied by two opposite pulse current alternately; the second one is constructed by two separate coils, each of

them having its own magnetizing circuit and pick-up circuit. Both of these schemes have disadvantages with respect to this principle [4]; the error of the single one comes from different operating time, the double coil's error source is the coil structure's difference. On the other hand, these sensors are difficult to be optimized. In order to improve the sensors properties, we put forward a novel structure; two coils wrapped on the same core, and connected in anti-series. The structure is novel in two ways. First, the sensor avoids the structural error based on the above principle. Second, this structure is simple and suitable for optimization. In this paper, we first introduce this sensor's structure. Then, we analyze the transient processing of the emf in coil, and find out the ideal testing point. After that, we put forward the optimizing techniques. At the end, the experimental results and its application in engineering testing show good agreement with the above analysis.

2 Principle

The principle of this kind of magnetic field sensor is illustrated in Fig. 1.

Coils 1 and 2 are two identical coils, which are wrapped over amorphous core, connected in anti-series; their joint terminal is connected at ground. Two identical pulse current sources $S_1 (I_1)$, $S_2 (I_2)$ supply coils 1 and 2, respectively. Therefore, the two coils are identical in structure and magnetize the amorphous core in opposite directions. According to the Faraday's law of induction, the emf in coil 1 is:

$$V_1 = -N \frac{d\phi_1}{dt} = -NA \frac{dB_1}{dt} = -NA \frac{d[\mu_0(H_1 + M_1)]}{dt} = -NA\mu_0 \left[1 + \frac{dM_1}{dH_1} \right] \frac{dH_1}{dt} \quad (1)$$

where ϕ is the magnetic flux of the amorphous core (Wb); $\mu_0 = 4\pi \times 10^{-7}$ (H/m) is the permeability of air; N is the turns of coils; A is the area of the amorphous core (m^2); B is the magnetic induction of the amorphous core (A/m); H is the magnetic field (A/m); M is the magnetization of the amorphous core (A/m).

Because

$$H_1 = H_{el} + H_d, \quad H_{el} = \alpha \frac{NI_1}{l_m}, \quad \frac{dH_{el}}{dt} \gg \frac{dH_d}{dt} \quad (2)$$

Here, H_d is the external (detected) magnetic-field (A/m); H_{el} is the magnetic-field induced by pulse-current I_1 (A/m); α is the revised factor of the leakage magnetic flux in air; l_m is the length of amorphous core (m).

Therefore

$$V_1 = -NA\mu_0 \left[1 + \frac{dM_1}{dH_1} \right] \frac{dH_{el}}{dt} = V_0 + \Delta V_1 = V_0 + V_0 \frac{dM_1}{dH_1} \quad (3)$$

Here, $V_0 = -NA\mu_0 (dH_{el}/dt)$, which is a constant parameter independent of the external magnetic field H_d ; we call it the zero magnetic-field voltage.

According to the same principle, the emf in coil 2 is:

$$H_2 = H_{el} - H_d, \quad H_{el} = \alpha \frac{NI_2}{l_m} = H_{el}$$

$$V_2 = -NA\mu_0 \left[1 + \frac{dM_2}{dH_2} \right] \frac{dH_{el}}{dt} = V_0 + \Delta V_2 = V_0 + V_0 \frac{dM_2}{dH_2} \quad (4)$$

As seen in Eq. (3) and Eq. (4), $V_0 (dM_1/dH_1)$ and $V_0 (dM_2/dH_2)$ reflect the change of H_d . Fig. 2 is the magnetic curve ($M-H$) of amorphous alloy. If the sensor's operating point is within the nonlinear range in the $M-H$ curve, especially when

$$M = aH + bH^2 \Rightarrow \frac{dM}{dH} = a + 2bH \quad (a, b \text{ are constants}) \quad (5)$$

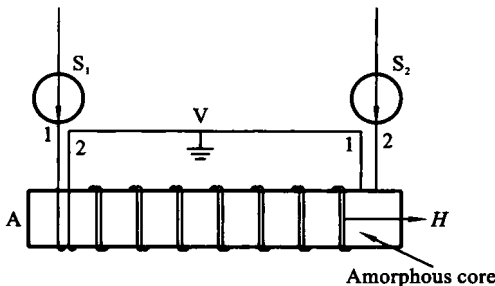


Fig. 1 The scheme of the double coil sensor

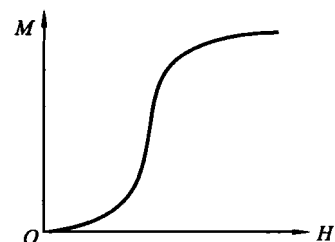


Fig. 2 The magnetic curve ($M-H$) of amorphous alloy

from Eq. (3) and Eq. (4) :

$$V_1 - V_2 = \Delta V_1 - \Delta V_2 = 2bV_0(H_1 - H_2) = -4bNA\mu_0 H_d \frac{dH_{el}}{dt} \quad (6)$$

From Eq. (6), we can get the signal of the external magnetic field H_d .

3 Signal's Pick-up

However, the emf in coil is changing complexly in one pulse cycle^[5], as shown in Fig. 3. Which is the best testing point and how to pick it up are two key clues in this sensor. We studied its transient processing deeply. The pulse current can be described as follows:

$$S(t) = \begin{cases} I_0(t), & nt_1 \leq t \leq nt_1 + t_0 \\ I_0(t) - I_0(t - t_0), & nt_1 + t_0 \leq t \leq (n+1)t_1 \end{cases} \quad (7)$$

$n=0,1,2,\dots$

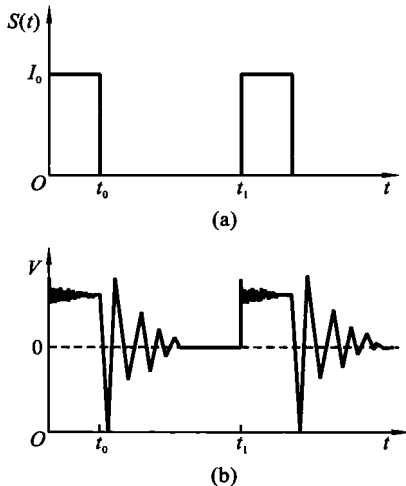


Fig. 3 The transient processing of the emf in coil

(a) The pulse current source $S(t)$; (b) The emf in pulse-reduction coil

Due to Eq. (6), the emf's transient processing can be divided into two periods.

(1) $nt_1 \rightarrow nt_1 + t_0$: the coil is excited by the pulse current, its emf arrives at its positive maximum rapidly, and the amorphous core reaches its operating point $H = H_e + H_d$ quickly; then the circuit goes into stability, and coil stores energy. During this processing, the amorphous core is induced by the induced magnetic field H_e and the external magnetic field H_d simultaneously. Both of these changes greatly affect the emf, therefore the change of H_d cannot be ignored; the emf is